A perturbed ghost model for estimating air-gun array signatures

Rob Telling and Sergio Grion, Shearwater GeoServices, UK*

Summary

We present an approach to air-gun array signature estimation that builds on the well-established method of solving for notional sources and seeks to take account of non-linear perturbations to the down-going wavefield, including attenuation of the ghost due to onset of cavitation. In current practice the effect on ghost amplitude is often described approximately via an assumed effective reflectivity at the sea-surface. Here, we describe perturbation of the ghost from the standard model by using a series of virtual notional sources situated in the water column, between the guns and the sea-surface. For the inversion problem to be well-posed in solving for these extra unknowns, additional near-field hydrophone measurements must be made. The advantage over the standard approach is a more accurate treatment of the ghost and no requirement to optimize model parameters. It is also found that the inversion is more stable than the alternative parameter-free approach that solves directly for real and mirror virtual notional sources. The improved performance and stability are demonstrated with a field data example.

Introduction

In marine seismic the formation of the sea-surface ghost on the source-side differs from that at the receiver-side due to the different scales of pressure amplitude. This is of the order of 10bar close to the source array, compared to subsurface reflections of order 10mbar at the receiver for a hard seabed at 1s two-way-time. The peak in positive pressure emitted by each gun is approximately reversed in sign on reflection at the sea-surface. If the magnitude of the reflected peak pressure combined from all guns exceeds the local ambient pressure, the water is put into tension, which can lead to transient cavitation. Cavitation is the emergence and growth of microscopic vapour bubbles and is typically observed in the context of underwater explosions (Cole, 1948, Medwin and Clay, 1998). A tension pulse exceeding the strength of water will perform work during the phase of rapid expansion of the cavitation ‘cloud’, leading to clipping of the pulse. The vapour bubbles in the cloud will then ultimately collapse as the tension falls, leading to a secondary event and emission of high frequencies (Landrø et al. 2011, Khodabandeloo and Landrø, 2018). The net effect is some loss of coherent down-going energy which is more noticeable at high frequencies. This helps explain why the observed interference from the source ghost is often smaller than expected, even when taking into account scattering from a rough sea (Kragh and Combee, 2000, Telling et al., 2018) and leads to estimation of reduced effective reflectivity at high frequency (Kyrvohuv and Campman, 2016, Ni et al., 2012).

Other non-linear behaviours that may take place in the near-field of the source array and lead to loss of energy include formation of a spray dome at the sea-surface, also called ‘shot effect’, that arises from the doubling of particle velocity on reflection. Wave propagation velocity is dependent on amplitude and this can lead to formation of shock fronts at high pressures, and energy loss due to heating. A contribution from these effects is not discounted, but they are relatively small compared to the onset of cavitation, which for a few milliseconds changes the state of the propagation medium.

Our standard approach to signature estimation is posed as an inversion with equal numbers of source elements and hydrophones and assumes a simple ghost model with reflection coefficient that varies with frequency according to a rough-sea scattering model (Telling et al., 2018). The forward model for data recorded at a given hydrophone in the near-field of the array is posed in the hybrid time-frequency domain (Hargreaves et al., 2015) as a linear algebraic sum of contributions from each notional source (Ziolkowski et al., 1982) and incorporates the relative motion of hydrophones and sources over time. Parkes and Hatton (1986) and Hampson (2017) propose to overcome the limitations of the simple ghost model by solving directly for the virtual notional sources that represent the ghost arrivals, in addition to the real notional sources. This removes the sea-surface reflectivity parameter from the inversion but requires making twice as many near-field hydrophone (NFH) measurements. Telling et al. (2018) describe a field test of this parameter-free method which gave promising results compared to the standard inversion but with a question mark over sensitivity to noise at low frequency and poorer de-bubble. A follow-up study into the noise sensitivity of the parameter-free method (Telling and Grion, 2019) found the inversion was less stable, mainly a result of the increased (virtual) source-receiver separation. This is most problematic at low frequencies due to the raised low frequency ambient noise profile typical of the near-surface layer of the ocean. While this can be overcome in practice using a frequency-split hybrid of the standard and parameter-free methods, an intrinsically more stable single inversion scheme would be desirable. Here we describe such a scheme, examine sensitivity to noise and test results on field data acquired with two NFH channels per source element.

Method

A flexible way to represent the non-linear interaction with the sea-surface is to position secondary virtual point sources in the water column between the guns and the sea-surface. The physical justification is that they represent the attenuation of the ghost due to cavitation and the subsequent signal from collapse of the cavitation cloud. The exact shape and size of the cavitation cloud is not known with precision and in practice will depend on gun configuration, sub-array separation and water-depth. The extent of the cloud will also be a function of time. We anticipate the origin to lie mid-way between sub-arrays, where superposition leads to the highest pressures and at a depth corresponding to where the ghost pulse magnitude exceeds ambient pressure. 2D finite-difference modelling (see Figure 1) suggests to us the initial location of the cavitation cloud is at a depth of around 3m and we used this depth, noting that at later times the simple propagation model will no longer hold. A more complete 3D analysis of the array incorporating the sub-array interaction would help to refine this initial estimate.

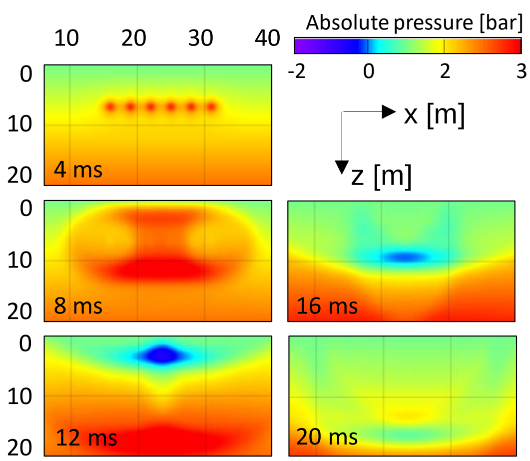

Figure 1: Snapshots from a 2D finite difference simulation of the acoustic wavefield for a six-element array (individual source peak level 2bar-m) linear in *x* and firing at 7m depth (*z*) below a perfectly reflecting flat sea-surface. Ambient depth-varying hydrostatic and atmospheric pressures are superimposed. Note the transient blue region showing net tension in the water.

Figure 2 illustrates the different configurations discussed here. The standard configuration solves for real notional sources and uses a simple parameterized ghost model which is optimized to minimize residual above the ghost notch (Telling et al., 2018). With the dual NFH configuration we can solve directly for both real and virtual notional sources without the need for prescribing reflectivity and hence call this 'parameter-free' (Hampson, 2017). The new scheme proposed here is similar to the standard case but with the addition of virtual sources in the water column that describe perturbation of the down-going wavefield. Furthermore we assume a simple deterministic ghost model with reflectivity as for the observed sea-state and do not optimize the parameters of this model. Analysis of sensitivity to noise was calculated using posterior covariance for our inverse problem the forward model for which, in the frequency domain, is given by:

$$\mathbf{d} = \mathbf{G}\mathbf{m} \qquad (1)$$

where $\mathbf{d}$ is a vector corresponding to the observed pressure data at each hydrophone position, $\mathbf{m}$ is a vector corresponding to the notional sources. $\mathbf{G}$ is a matrix operator which describes the propagation of acoustic energy from each source element to each hydrophone. Matrix elements are comprised of a geometric scaling term $1/r$ and a phase shift based on the delay time $\exp(-i\omega r/c)$ where r is the distance from a given source element to a given hydrophone and c the sound speed in water.

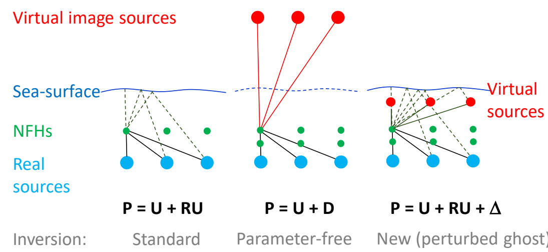

Figure 2: Schematic of the different inversion scheme geometries. The standard case is based on a single NFH per source element and where real notionals are the unknowns to be solved for. Parameter-free inversion is based on two NFH per source element solving for both real (blue) and virtual (red) sources. The new scheme is similar to the standard but with the addition of virtual sources in the water column that describe perturbation of the wavefield.

The time-dependence of r due to relative motion of bubble and hydrophone is handled in between inverse and forward Fourier transforms. This is implemented for the real and virtual image notional sources but not the virtual sources in the water column which represent the perturbation to the ghost. Cavitation does not last more than a few 10s of milliseconds, so their contribution to the wavefield is assumed to occur from points fixed in space. The posterior covariance for a given $\mathbf{G}$ is:

$$\tilde{\mathbf{C}}_\mathbf{m} = \left(\mathbf{G}^{*}\mathbf{C}_\mathbf{d}^{-1}\mathbf{G} + \mathbf{C}_\mathbf{m}^{-1}\right)^{-1} \qquad (2)$$

(Tarantola 2005), where the prior covariance matrices for the observed data, $\mathbf{C}_\mathrm{d} = \sigma_d^2\mathbf{I}$, and for the model, $\mathbf{C}_\mathrm{m} = \sigma_m^2\mathbf{I}$, are assumed to be diagonal and where σ_d and σ_m are their respective standard deviations, $\mathbf{I}$ is the identify matrix and the * denotes complex conjugate transpose. The posterior standard deviation of the model, $\tilde{\sigma}_m$ is then the square-root of the diagonal of the resulting covariance matrix. In the next section, we use (2) to calculate noise sensitivity for the various inversion schemes. For this purpose, we assume priors $\sigma_d = 0.01$ at 0 Hz, reducing with frequency according to the simplified trend for observed ambient noise given in Figure 3 and σ_m= 1.0.

The field data example used to test each inversion scheme uses a source with two sub-arrays. A schematic plan of the array is provided in Figure 4. The source elements are positioned at 7m depth and near-field hydrophone channels are at 6m and 4m depth and co-located in *x* and *y* for each source element. For the signature modelling we use measured coordinates for each source element on a shot by shot basis and derive *x* and *y* positions from the two R-GPS receivers on each float. The *z* position is provided directly from the gun depth sensors.

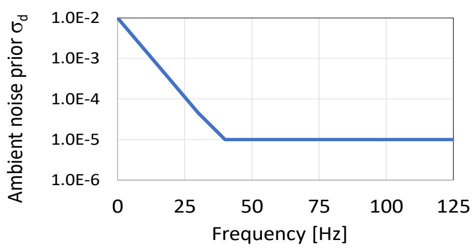

Figure 3: σ_d assumed for the analysis of sensitivity to noise for the different inversion schemes. This simplified profile is taken from a NFH noise recording.

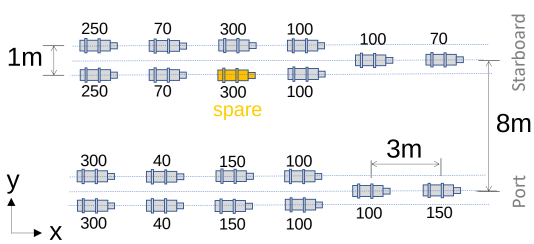

Figure 4: Source array nominal configuration comprising guns of type Teledyne Bolt Model 1500LL or 1900LLXT with capacities in the range 40-300in^3. Total volume 2740in^3. Coordinate *x* increases with distance away from vessel.

We apply de-signature to the seismic data in τ-p, using directional filters derived from each set of far-field wavelets for take-off angles in the range -30° to +70°. This process encapsulates source de-ghosting, de-bubble and matching to a zero-phase Ormsby wavelet.

Results – Theoretical sensitivity to noise

Figure 5 shows the result of the noise sensitivity analysis for the new inversion scheme, compared against the standard and parameter-free cases. Higher sensitivity to noise is apparent at the end of the array where the relative motion of source and hydrophone leads to poorer hydrophone coverage. Figure 6 is a line plot summary at the position of black lines in Figure 5. The parameter-free inversion is clearly problematic for virtual sources at lower frequencies (<40Hz) and in comparison, the new inversion is much less sensitive to noise. This is largely due to reduced separation of the notional sources and NFHs. Also, the perturbed signal is predominantly a high frequency contribution (see Figure 7), so low frequency sensitivity is less critical for the new method.

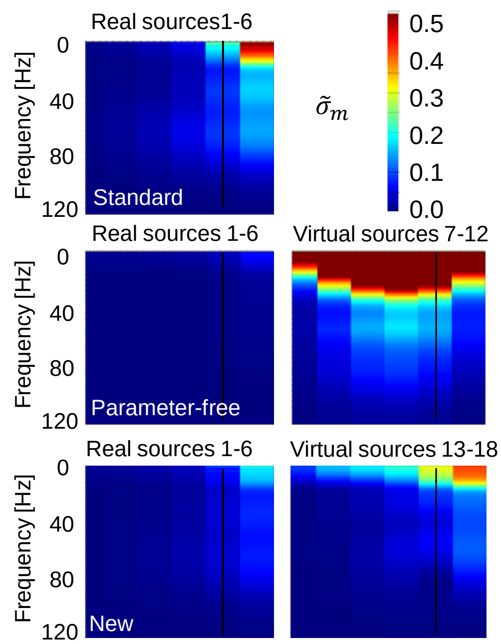

Figure 5: $\tilde{\sigma}_m$ for real notional sources 1-6 (starboard sub-array, numbering increasing with *x*) at 7m depth, virtual sources 7-12 at image locations above the sea surface (-7m) and virtual notional sources 13-18 at 3m below the sea-surface. The analysis was run for the time varying geometry for 1s duration.

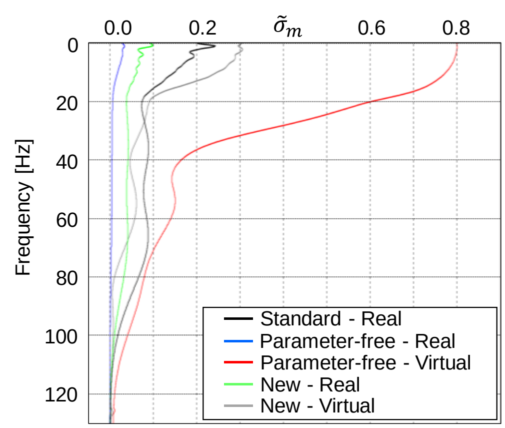

Figure 6: Summary line plots of $\tilde{\sigma}_m$ from Figure 5 (black lines).

Results - Data example

Figure 7 shows an example of the estimated notional sources for one shot obtained via the new inversion scheme, including the virtual sources representing the perturbed ghost. Note the almost complete absence of bubble signature for these virtual sources, indicating that they are describing only the high-frequency perturbation of the ghost. Figure 8 shows the corresponding derived far-field signatures and a comparison against those for the standard and parameter-free inversion schemes. We see the initial arrivals are comparable, but Figure 9 highlights the issue with bubble oscillation for the parameter-free inversion.

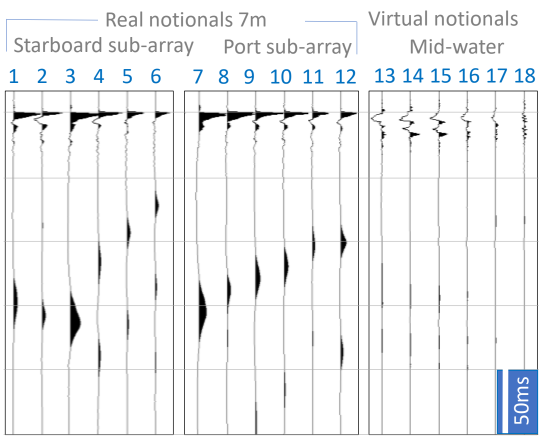

Figure 7: Example notional sources solved via the new inversion. Sources 1-12 are located at the source element coordinates. Sources 13-18 represent the ghost perturbation and are located mid-way between sub-arrays at 3m depth.

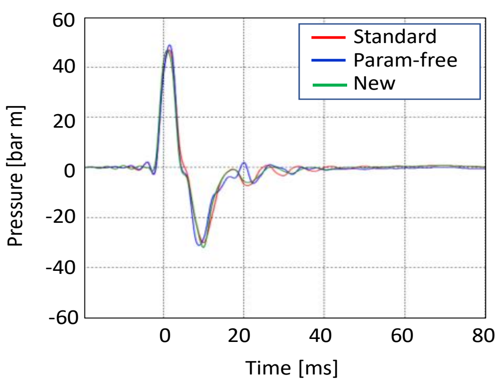

Figure 8: Vertical far-field signature showing reduced amplitude ghost and comparable initial arrivals for the three inversion schemes.

Figure 10 shows the results from de-signature processing. For each scheme the ghost removal appears artefact free as observed near the water-bottom. However, it is clear that the parameter-free inversion mishandles bubble pulse deconvolution, which is most apparent on the direct arrival.

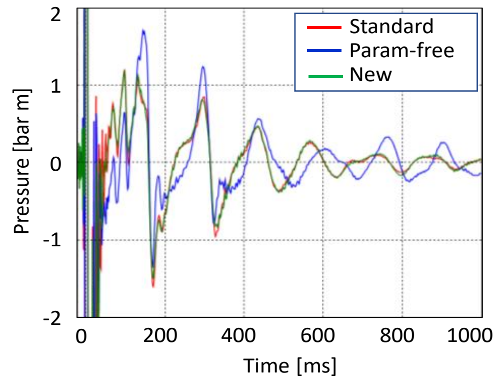

Figure 9: Vertical far-field signature showing bubble oscillation.

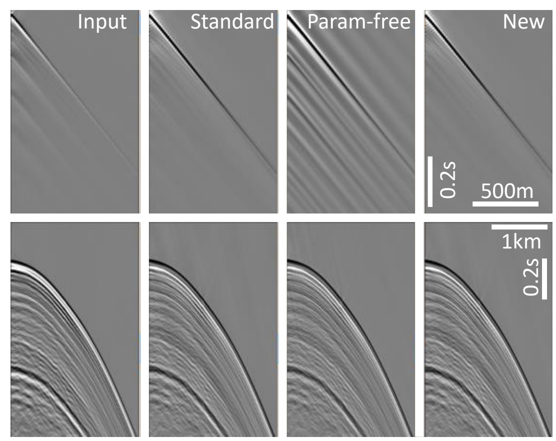

Figure 10: Example shot record before and after de-signature for the three inversion schemes. Top sequence: zoom on the direct arrival, lower sequence: zoom close to the seabed, at 3s TWT.

Conclusions

We have described an inversion scheme that incorporates perturbation of the source ghost due to non-linear phenomena and have applied this to the de-signature of field data. The derived far-fields and de-signature results were of good quality and free of artefacts. The method is based around solving for additional sources in the water column between sub-arrays and hence requires additional NFH measurements. However, the scheme has the advantage over the standard approach in that it better represents the physics at the source array and does not require parameter-fitting or optimization of the frequency-varying reflectivity to be carried out. It also does not suffer the high sensitivity to noise observed for the parameter-free dual NFH method, requires fewer virtual sources, and is conceptually simpler than a hybrid of the standard and parameter-free methods.

References

Cole, R. H. [1948]. Underwater Explosions, Princeton University Press, New Jersey

Hampson, G. [2017]. Notional ghosts. 86th Annual SEG Meeting Expanded Abstracts

Hargreaves, N., Grion, S. and Telling, R. [2015]. Estimation of air-gun array signatures from near-gun measurements - least-squares inversion, bubble motion and error analysis. 85th SEG Meeting Expanded Abstracts, 149-153.

Khodabandeloo, B. and Landrø M. [2018]. Acoustically induced cavity cloud generated by air-gun arrays – comparing video recordings and acoustic data to modeling. J. Acoust. Soc. Am. 143 (6) 3383-3393.

Kragh, E., and Combee, L. [2000]. Using a seismic reflector for resolving streamer depth and sea surface profiles, First Break, 18, 463-467

Kryvohuz, M. and Campman, X. [2016]. Optimization of sea surface reflection coefficient and source geometry in conventional dual source flip/flop marine seismic acquisition 86th SEG Meeting Expanded Abstracts, 188-192.

Landrø, M., Amundsen, L. and Barker, D. [2011]. High frequency signals from air-gun arrays. Geophysics 76 (4) Q19-Q27

Medwin, H. and Clay, C. S. [1998]. Fundamentals of Acoustical Oceanography. Academic Press, London.

Ni, Y., Niang, C., Siliqi, R. [2012]. Monitoring the stability of airgun source array signature. 82nd Annual SEG Meeting, Expanded Abstracts, 1-5

Parkes, G. and Hatton, L. [1986] The Marine Seismic Source. D. Reidel, Dordrecht

Telling, R., Light, R., Grion, S., Denny, S. and Williams, R. G. [2018] Signature estimation and drop-out implications for a triple source marine seismic survey, 80th EAGE Conference and Exhibition, Extended Abstracts

Telling, R. and Grion, S. [2019] Signature estimation using dual near-field hydrophones: sensitivity to noise and a proposed hybrid methodology, 81st EAGE Conference and Exhibition, Extended Abstracts

Ziolkowski, A., Parkes, G., Hatton, L. and Haugland T. [1982]. The signature of an air gun array: Computation from near-field measurements including interactions. Geophysics, 47 (10), 1413-1421.